metals

MDPI

Article

Peculiarities of the Electro- and Magnetotransport in Semimetal $MoTe_2$

Alexandra N. Perevalova *, Sergey V. Naumov and Vyacheslav V. Marchenkov

M.N. Mikheev Institute of Metal Physics, UB RAS, 620108 Ekaterinburg, Russia
* Correspondence: domozhirova@imp.uran.ru

Abstract: Weyl semimetal $MoTe_2$ single crystal was grown by the chemical vapor transport method. Electrical resistivity, magnetoresistivity, and Hall effect in $MoTe_2$ were studied in detail. It was shown that both the electrical resistivity in the absence of a magnetic field and the conductivity in the field depend on temperature according to a quadratic law in a wide temperature range. It has been suggested that the quadratic temperature dependence of the conductivity in a magnetic field at low temperatures might be associated with the "electron-phonon-surface" interference scattering mechanism. The analysis of data on the Hall effect in $MoTe_2$ was carried out using single-band and two-band models. Apparently, the two-band model is preferable in such systems containing different groups of current carriers.

Keywords: Weyl semimetal $MoTe_2$; resistivity; Hall effect; quadratic temperature dependence

Citation: Perevalova, A.N.; Naumov, S.V.; Marchenkov, V.V. Peculiarities of the Electro- and Magnetotransport in Semimetal $MoTe_2$. *Metals* **2022**, *12*, 2089. https://doi.org/10.3390/met12122089

Academic Editors: Daria V. Lazurenko and Michael R. Koblischka

Received: 30 September 2022
Accepted: 28 November 2022
Published: 6 December 2022

1. Introduction

In recent years, topological materials have attracted a lot of attention because they have a non-trivial topology of the electronic band structure and unusual electronic properties. In addition to interest from the point of view of fundamental science, such materials are actively studied due to the possibility of their practical application in micro-, nanoelectronic and spintronic devices. Topological materials include topological semimetals [1,2] as well as previously discovered topological insulators [3,4]. Topological insulators have an energy gap in the bulk and topologically protected gapless surface states. At the same time, topological semimetals have unusual states both on the surface and in bulk. Such materials include Weyl semimetals [5]. In the bulk of a Weyl semimetal, two nondegenerate bands with linear dispersion cross near the Fermi level, forming Weyl nodes, which always exist in pairs with opposite chirality. Quasiparticles near such nodes behave such as massless Weyl fermions in high-energy physics. Similar to topological insulators, Weyl semimetals have topologically protected surface states called Fermi arcs. They are open curves in momentum space that connect the projections of bulk Weyl nodes with opposite chirality on the surface.

Weyl fermions can only be found in crystals in which either inversion symmetry or time-reversal symmetry is broken. The existence of such quasiparticles was first experimentally confirmed in TaAs in 2015 [6]. Soon, the authors of [7] predicted another type of band crossing with a tilted Weyl cone. As a result, the Lorentz invariance is violated, and the corresponding quasiparticles are called type-II Weyl fermions. Instead of the point-like Fermi surface in a type-I Weyl semimetal, the type-II Weyl node is the touching point between electron and hole pockets. The authors of [7] also theoretically predicted that the WTe_2 compound is a type-II Weyl semimetal. This was experimentally confirmed in [8,9]. By analogy with WTe_2, it was theoretically predicted [10] and experimentally confirmed [11] that $MoTe_2$ is also a type-II Weyl semimetal.

WTe_2 and $MoTe_2$ belong to a large group of materials, layered transition metal dichalcogenides, with the general chemical formula MX_2, where M is a transition metal atom, and X

is a chalcogen atom [12]. However, unlike WTe_2, for which the orthorhombic structure Td is stable with temperature, $MoTe_2$ can crystallize into one of three phases: hexagonal (2H), monoclinic (1T′), or orthorhombic (Td) [13]. Depending on the synthesis conditions, $MoTe_2$ can be obtained in the hexagonal (2H) or monoclinic (1T′) phase, which is also called the α- and β-phase, respectively [14]. The 2H-phase (space group $P6_3/mmc$) is semiconducting. Whereas the 1T′-phase is semimetallic and belongs to the centrosymmetric space group $P2_1/m$. A temperature-induced phase transition from the high-temperature 1T′-phase (β-$MoTe_2$) to the low-temperature Td-phase of $MoTe_2$ near 250 K was reported in [15]. The Td-phase has a similar crystal structure in the layer plane as the 1T′-phase but has a vertical (90°) packing and belongs to the noncentrosymmetric space group $Pmn2_1$. It is in Td-phase that $MoTe_2$ is a type-II Weyl semimetal [10,11].

Due to the unusual topology of the electronic band structure, Weyl semimetals have unique electronic transport properties. Such features of electronic transport include extremely large unsaturated magnetoresistance [16,17], negative longitudinal magnetoresistance [18], low effective mass and ultrahigh mobility of current carriers [19,20], the intrinsic anomalous Hall effect, etc. In addition, quadratic temperature dependence of the electrical resistivity was observed in $MoTe_2$ [21–23] and WTe_2 [24,25] single crystals in a very wide temperature range. In particular, it was found in [21] that the electrical resistivity of semimetallic $MoTe_2$ depends on temperature according to a quadratic law in the temperature range from 1.7 to 50 K. It was suggested (see [21] and references therein) that, in addition to electron-electron scattering, other possible scattering mechanisms can lead to the T^2-dependence of the electrical resistivity of $MoTe_2$; in particular, the contribution proportional to T^2 can be associated with electron-phonon scattering, as this was shown for a semiconductor TiS_2 compound [26]. However, further research is required to understand the role of all scattering mechanisms in $MoTe_2$. As we previously showed for the WTe_2 single crystal in [23], not only the electrical resistivity in the absence of a magnetic field but also the conductivity in the field depends on temperature according to a quadratic law in a wide temperature range from 12 K to ~70 K and ~55 K, respectively. Therefore, it is of interest to determine how the resistivity (conductivity) of $MoTe_2$ in a magnetic field depends on temperature. In addition, when analyzing data on the Hall effect in topological semimetals, a single-band [19] or two-band model [27,28] is usually used. In [25], we showed that the estimates of the concentrations and mobilities of current carriers in WTe_2 obtained using these two models are in good agreement with each other at 12 K. It is of interest to carry out such a comparison in a wider temperature range, in particular, using $MoTe_2$ as an example.

This paper is devoted to the study of the features of the electro- and magnetotransport of the Weyl semimetal $MoTe_2$ single crystal in order to establish the form of the temperature dependence of the resistivity (conductivity) in a magnetic field, compare the results of using single-band and two-band models to analyze its magnetotransport characteristics.

2. Materials and Methods

$MoTe_2$ single crystal was grown by chemical vapor transport method [29] using bromine as a transport agent. Powders of molybdenum and tellurium in a stoichiometric ratio, as well as bromine, whose vapor density was 5 mg/cm^3, were sealed into a quartz ampoule evacuated to a residual pressure of ~10^{-4} atm. Then the ampoule was placed into a horizontal tube furnace with a linear temperature gradient, where the temperatures T_1 ("hot" zone) and T_2 ("cold" zone) were 850 °C and 770 °C, respectively. The process of growing a single crystal was carried out for 500 h, followed by slow cooling to room temperature. It is known that $MoTe_2$ undergoes a structural transition from the semiconductor α-phase to the metallic β-phase at a temperature of 820 °C for tellurium-rich samples and 880 °C for molybdenum-rich ones [14]. Therefore, the ampoule containing the grown crystal and evacuated to 10^{-4} atm. was heated to 910 °C and held for 3 h. In order to obtain the high-temperature phase, the quartz ampoule with crystal was rapidly cooled to room temperature by water quenching.

The grown crystal was investigated using X-ray diffractometer DRON-2.0 (Joint Stock Company "Bourevestnik", Saint Petersburg, Russia.) with CrKα radiation. Fragments of the X-ray diffraction pattern taken from the surface of the sample immediately after growth, as well as after quenching, are shown in Figure 1a. Since all peaks can be indexed as (00*l*), the surface of the single crystal under study coincides with the (001) type plane. It can be seen that the intensity ratio of the lines from the (00*l*) planes changed after quenching. Note also that the lattice parameter *c* changed significantly from 13.93 ± 0.01 Å for the as-grown crystal to 13.81 ± 0.01 Å for the quenched one. The value of the lattice parameter *c* was estimated from the position of the (006) line. Figure 1b clearly shows the shift of the (006) line towards larger angles for the quenched sample. The obtained values of *c* before and after quenching are close to the values of lattice constant *c* for α-$MoTe_2$ (hexagonal lattice) and β-$MoTe_2$ (monoclinic lattice), respectively [14,30,31]. These results indicate a structural phase transition that occurred in $MoTe_2$. The chemical composition of the sample was studied by energy-dispersive X-ray microanalysis using an Quanta 200 Pegasus scanning electron microscope (FEI Company, Eindhoven, the Netherlands) with an EDAX attachment at the Collaborative Access Center "Testing Center of Nanotechnology and Advanced Materials" of M.N. Mikheev Institute of Metal Physics of the Ural Branch of the Russian Academy of Sciences (IMP UB RAS). The chemical composition of the single crystal corresponds to stoichiometric $MoTe_2$.

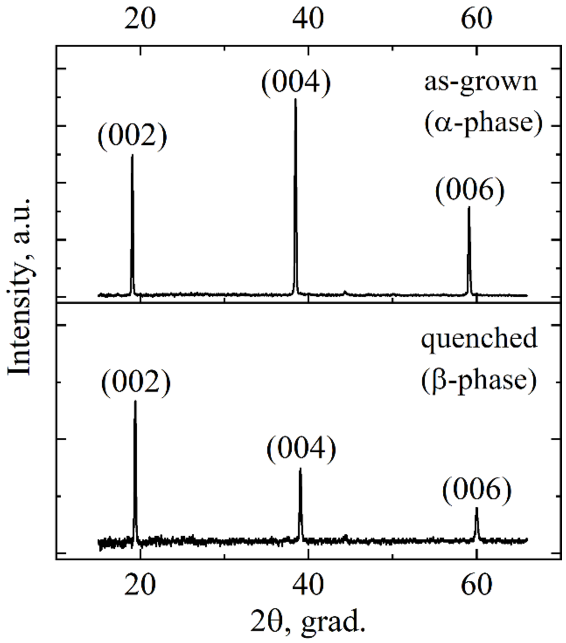

(**a**)

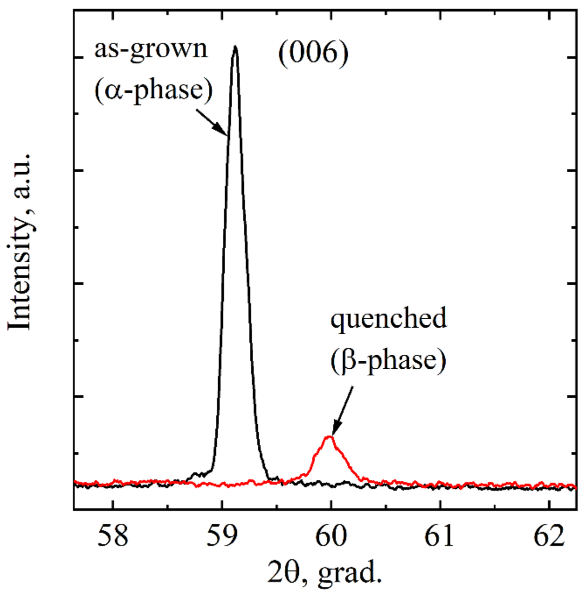

(**b**)

Figure 1. Fragments of X-ray diffraction patterns taken from the surface of the $MoTe_2$ single crystal: (**a**) The as-grown single crystal corresponds to α-$MoTe_2$; The single crystal quenched from 910 °C corresponds to β-$MoTe_2$; (**b**) Change of lattice parameter *c* of $MoTe_2$ after quenching.

In this paper, we studied the quenched $MoTe_2$ single crystal, which corresponded to the β-phase at room temperature and had the shape of a thin plate with dimensions ~6 × 1 × 0.2 mm^3. The resistivity and Hall effect were measured by the four-contact method in the temperature range from 4.2 K to 290 K and in magnetic fields up to 9 T on a PPMS-9 setup (Quantum Design, San Diego, CA, USA) at the Collaborative Access Center "Testing Center of Nanotechnology and Advanced Materials" of IMP UB RAS. During the measurements, the electric current flowed in the (001) type plane, and the magnetic field was directed along the *c* axis, i.e., perpendicular to the plane of the plate. The residual resistivity ratio (RRR) in our sample is $\rho_{300\,K}/\rho_{4.2\,K} \approx 15$, which is comparable to the RRR value in [21], but at the same time, much lower than the RRR in [27], which indicates a large number of defects in the crystal under study. For the convenience of interpretation, some of the experimental results obtained are presented in the form of conductivity $\sigma_{xx} = [\rho(B) - \rho(0)]^{-1}$, where $\rho(B)$ is the resistivity in magnetic field B.

3. Results and Discussion

3.1. Electrical Resistivity

The temperature dependence of the electrical resistivity $\rho(T)$ of $MoTe_2$, measured in the temperature range from 4.2 K to 290 K, is shown in Figure 2. It can be seen that the dependence $\rho(T)$ has a "metallic" type, where ρ increases from 0.29×10^{-4} Ohm·cm to 4.2×10^{-4} Ohm·cm with increasing temperature. The $\rho(T)$ curve shows a weak feature at a temperature of ~260 K. A similar behavior of the electrical resistivity near 250 K was observed in [21–23,27] and is associated with the structural phase transition from the monoclinic 1T′-phase (β-$MoTe_2$) to the orthorhombic Td-one, which was reported in [15]. The inset shows the dependence $\rho = f(T^2)$. It can be seen that in the temperature range from 4.2 K to 45 K, the dependence $\rho(T)$ can be represented as $\rho = \rho_0 + AT^2$. The coefficient A is 2.8×10^{-8} Ohm·cm·K^{-2} in our case, which coincides in order of magnitude with the value of 1.54×10^{-8} Ohm·cm·K^{-2} given in [21], where a quadratic temperature dependence of the electrical resistivity of $MoTe_2$ was also observed in the temperature range from 1.7 to 50 K. Such a dependence $\rho(T)$ at temperatures below ~10–15 K is usually explained by electron-electron scattering with a collision frequency proportional to T^2. At higher temperatures, the electron-phonon scattering mechanism usually dominates. In this case, at $T << \Theta_D$ (Θ_D is the Debye temperature), the dependence $\rho(T)$~T^5 can be observed, and at temperatures comparable to Θ_D, $\rho(T)$ is linear. In [27,32], where the transport characteristics of semimetallic $MoTe_2$ were also studied, the data on the temperature dependence of the electrical resistivity were fitted, and it was found that there is a contribution to the resistivity proportional to T^5. At the same time, for our crystal, as in [21–23], no contribution of ~T^5 to the resistivity is observed at $T << \Theta_D$, where Θ_D = 135 K was taken from [23].

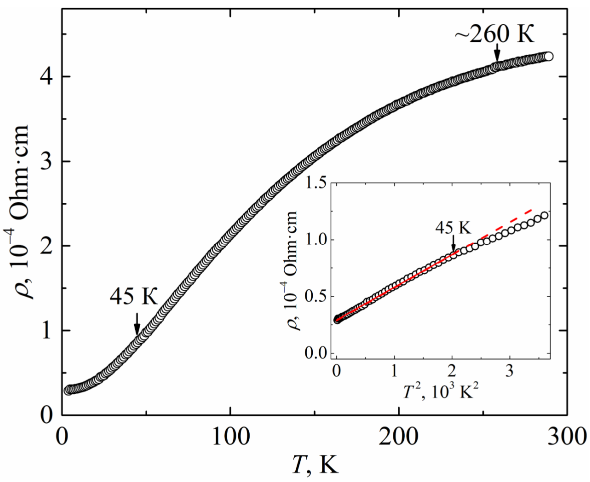

Figure 2. Temperature dependence of the electrical resistivity of $MoTe_2$ in the temperature range from 4.2 K to 290 K. The inset shows the dependence $\rho = f(T^2)$ at temperatures from 4.2 K to 60 K.

The quadratic temperature dependence of the electrical resistivity in a wide temperature range was also observed in pure metals. Thus, tungsten single crystals were studied in the temperature range from 2 to 40 K in [33], where another mechanism was proposed that leads to the T^2-dependence $\rho(T)$, called the "electron-phonon-surface" interference scattering mechanism. In addition, the quadratic temperature dependence of resistivity (conductivity) in a magnetic field was observed in tungsten single crystals under conditions of the static skin effect [34]. In [25], we found that in the Weyl semimetal WTe_2 single crystal, both the electrical resistivity in the absence of a magnetic field and the conductivity in a field depend on temperature according to a quadratic law in a wide temperature range from 12 K to ~70 K and ~55 K, respectively. By analogy with WTe_2, it can be expected that the quadratic dependence of the resistivity (conductivity) of $MoTe_2$ should also be observed in the presence of a magnetic field.

3.2. Resistivity (Conductivity) in Magnetic Field

Figure 3 shows the temperature dependence of the conductivity $\sigma_{xx} = [\rho(B) - \rho(0)]^{-1}$ of the $MoTe_2$ single crystal in a magnetic field of 9 T in the temperature range from 4.2 to 60 K. The inset shows the conductivity as $\sigma_{xx} = f(T^2)$. It can be seen that the value of σ_{xx} varies with temperature according to the quadratic law σ_{xx} = const + CT^2 in a wide temperature range from 4.2 K to 60 K. In this case, two temperature ranges can be distinguished, namely (4.2–20) K and (20–60) K, where the coefficient C is 32.6 $\mathrm{Ohm^{-1} \cdot cm^{-1} \cdot K^{-2}}$ and 79.2 $\mathrm{Ohm^{-1} \cdot cm^{-1} \cdot K^{-2}}$, respectively. A similar change in the coefficients at T^2 was observed by the authors of [33], where the electrical resistivity of tungsten single crystals was studied, and it was shown that the quadratic-in-temperature contribution to the resistivity at low temperatures is due to the scattering of conduction electrons by the sample surface, where the "electron-phonon-surface" interference scattering mechanism takes place. In addition, it was shown in [34] that in tungsten single crystals under conditions of a static skin effect, the conductivity in the magnetic field depends on temperature according to a quadratic law, which is also associated with the "electron-phonon-surface" scattering mechanism. Therefore, it can be assumed that the quadratic temperature dependence of σ_{xx} observed at temperatures from 4.2 K to 20 K in our single crystal might be associated with the "electron-phonon-surface" interference scattering mechanism [30,31]. In order to verify this, further studies are required, in particular, measurements of the resistivity of "sized" crystals (see, for example, [35] and references therein). Whereas the T^2-dependence of the conductivity in a magnetic field from ~20 K to 60 K seems to be associated with contributions from various scattering mechanisms, primarily from the specific electron-phonon scattering process leading to T^2.

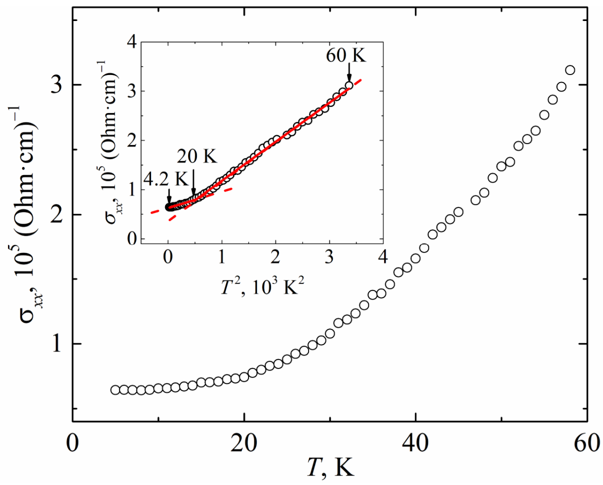

Figure 3. Temperature dependence of the conductivity of $MoTe_2$ in a magnetic field of 9 T in the temperature range from 4.2 K to 60 K. The inset shows the dependence $\sigma_{xx} = f(T^2)$ at temperatures from 4.2 K to 60 K.

3.3. Hall Effect

The analysis of data on the Hall effect in the $MoTe_2$ single crystal under study was carried out in the framework of a single-band model. In order to calculate the Hall coefficient R_H, concentration n, and mobility μ of main charge carriers, the following equations were used.

$$R_H = \frac{\rho_H}{B}, \quad (1)$$

$$n = \frac{1}{R_H \cdot e}, \tag{2}$$

$$\mu = \frac{R_H}{\rho}, \tag{3}$$

where ρ_H is the Hall resistivity; B is the magnetic field induction; e is the electron charge; ρ is the electrical resistivity in the absence of a magnetic field. Figure 4 shows the temperature dependences of R_H, n, and μ in the $MoTe_2$ single crystal. Since R_H is negative, electrons are the majority of charge carriers. Their concentration and mobility at a temperature of 4.2 K are 2.6×10^{20} cm^{-3} and 0.8×10^3 cm^2/(V·s), respectively. The value of n slightly changes with temperature. At the same time, the mobility μ decreases strongly with temperature, which can be explained by an increase in the scattering efficiency.

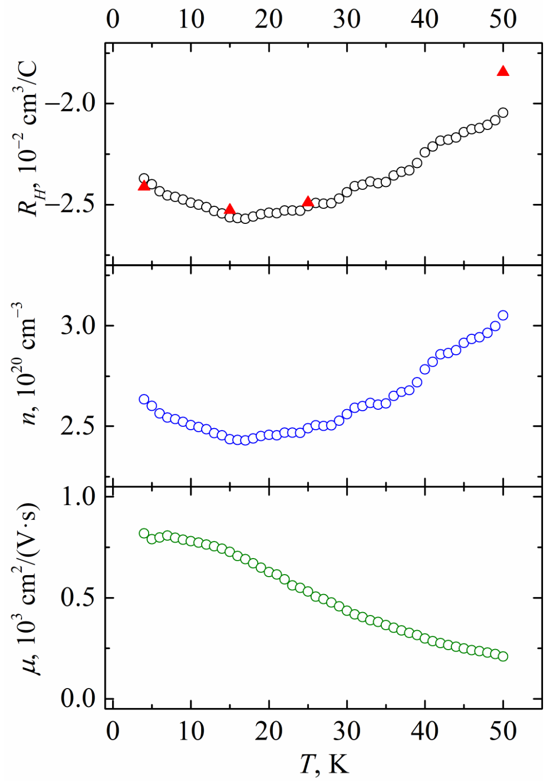

Figure 4. Temperature dependences of the Hall coefficient R_H, concentration n, and mobility μ of current carriers in $MoTe_2$, obtained using the single-band model in a field B = 9 T. The red triangles show the values of the Hall coefficient obtained on the basis of the two-band model.

At the same time, it is known that $MoTe_2$ contains carriers of both electron and hole types [10,11]. In such systems, the field dependences of the resistivity ρ in a magnetic field and Hall resistivity ρ_H are usually analyzed using a two-band model. In this case, the equations for ρ and ρ_H can be written in the form presented in [36]:

$$\rho = \frac{1}{e}\frac{(n_h\mu_h + n_e\mu_e) + (n_h\mu_e + n_e\mu_h)\mu_h\mu_e B^2}{(n_h\mu_h + n_e\mu_e)^2 + (n_h - n_e)^2\mu_h^2\mu_e^2 B^2}, \tag{4}$$

$$\rho_H = \frac{B}{e}\frac{(n_h\mu_h^2 - n_e\mu_e^2) + (n_h - n_e)\mu_h^2\mu_e^2 B^2}{(n_h\mu_h + n_e\mu_e)^2 + (n_h - n_e)^2\mu_h^2\mu_e^2 B^2}, \tag{5}$$

where n_e (μ_e) and n_h (μ_h) are the concentration (mobility) of electrons and holes, respectively.

Figure 5a shows the field dependences of the resistivity $\rho(B)$ in a magnetic field and Hall resistivity $\rho_H(B)$ of the $MoTe_2$ single crystal at temperatures of 4.2 K, 15 K, 25 K, and 50 K. The solid red lines correspond to fitting curves obtained using Equations (4) and (5) within the framework of the two-band model. It can be seen that the experimental data are well described by the fitting curves. The obtained values of the concentrations and mobilities of electrons and holes depending on the temperature are shown in Figure 5b. The values of n_e are of the order of 10^{20} cm^{-3} and vary slightly with temperature, which is consistent with the data obtained within the single-band model (Figure 4). At the same time, the hole concentration n_h decreases drastically with increasing temperature above 25 K. The electron mobility μ_e decreases with increasing temperature over the entire temperature range studied, as in the case of the single-band model. Whereas the hole mobility μ_h decreases with increasing temperature up to 25 K, at higher temperatures, an increase in the value of μ_h is observed. At T = 4 K, the values of μ_e and μ_h are 1.10×10^3 cm^2/(V·s) and 0.58×10^3 cm^2/(V·s), respectively. The geometric-mean mobility $\mu = \sqrt{\mu_e \mu_h}$ is in good agreement with the carrier mobility obtained within the single-band model. It can be seen that the values of the concentration n_e and mobility μ_e of electrons mainly exceed the values of n_h and μ_h of holes. This means that electrons are the main type of carriers, which also agrees with the single-band model. Note that, in our case, the carrier mobility, according to the estimates made, is an order of magnitude lower than, for example, in [27]. Apparently, this is due to a large number of defects in our crystal and a lower RRR. At the same time, the qualitative behavior of the obtained n_e (μ_e) and n_h (μ_h) are in good agreement with the results given in [22,27], where the two-band model was used. In addition, theoretical calculations of the electronic structure at various temperatures were carried out in [22], and it was shown that at temperatures below 35 K, electron-hole compensation is observed in Td-MoTe$_2$, whereas at higher temperatures, the Fermi surface is reconstructed mainly due to a decrease in the volume of hole pockets. This agrees with our results presented in Figure 5b, where at temperatures from 4.2 to 25 K $n_e \approx n_h$, while at higher temperatures, the hole concentration n_h strongly decreases.

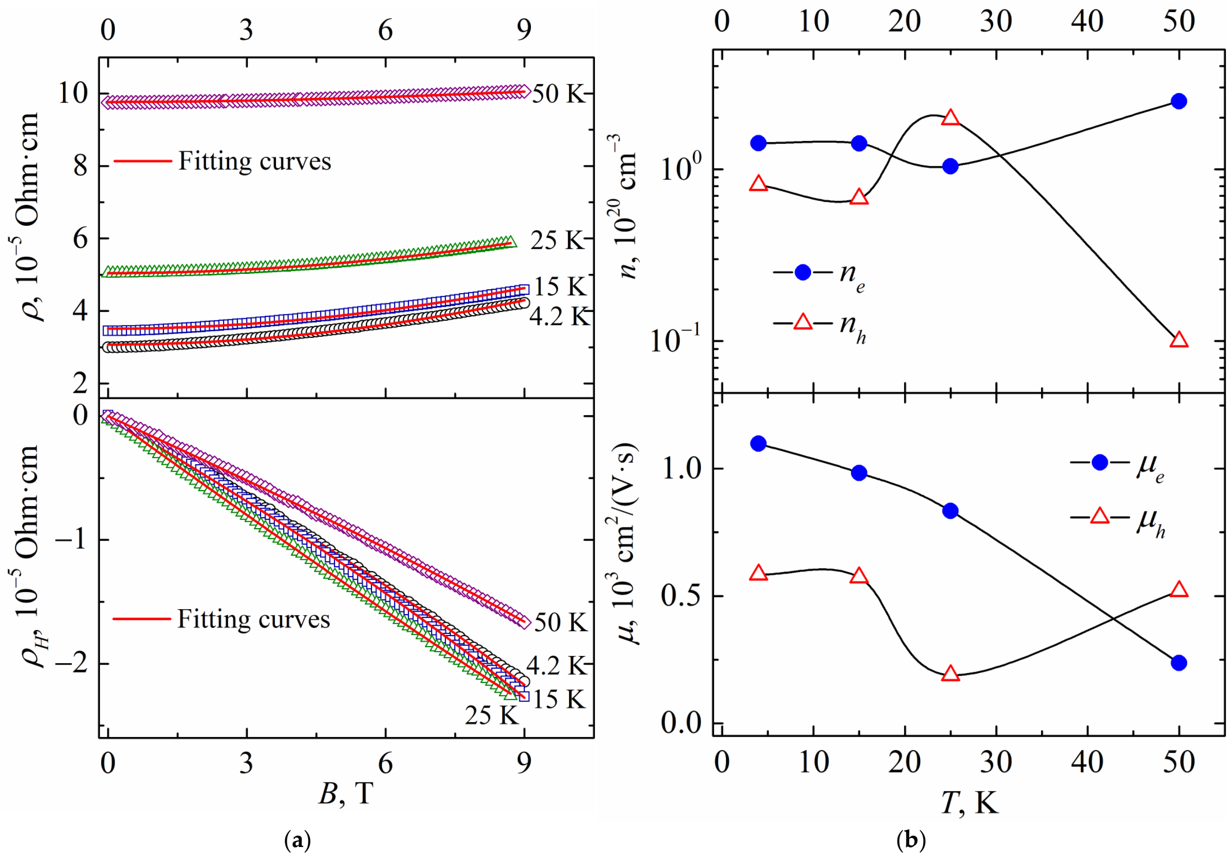

Figure 5. Analysis of data on the Hall effect in MoTe$_2$ using a two-band model: (**a**) Field dependences of the Hall resistivity $\rho_{\mathrm{H}}(B)$ (lower curve) and resistivity ρ (B) (upper curve) in a magnetic field for

$MoTe_2$ at temperatures of 4.2 K, 15 K, 25 K, and 50 K. Open symbols are experimental data; solid red lines are fitting curves obtained using the two-band model; (**b**) Temperature dependences of the concentration and mobilities of electrons and holes obtained on the basis of the two-band model.

In [25], the concentrations and mobilities in WTe_2 were also estimated using single-band and two-band models. It was shown that the values of concentrations and mobilities obtained using both models are in good agreement with each other. In [25] the Hall coefficient was calculated using the two-band model. The obtained value of R_H is in good agreement with the value obtained from the experimental data based on the single-band model. Therefore, the Hall coefficient was also calculated for $MoTe_2$ using the two-band model. The values obtained at temperatures of 4.2 K, 15 K, 25 K, and 50 K are plotted in Figure 4. It can be seen that the Hall coefficients calculated for both models are in good agreement. Apparently, this may indicate that the two-band model is applicable to systems similar to $MoTe_2$, containing different groups of charge carriers that differ in sign, mobility, etc. Moreover, the two-band model is preferable to the single-band one.

4. Conclusions

1. The quadratic temperature dependence of the electrical resistivity of $MoTe_2$ was observed in a wide temperature range from 4.2 K to 45 K, which is consistent with the experimental results previously reported.
2. The quadratic temperature dependence of the conductivity in a magnetic field was found in a wide temperature range. Moreover, two intervals can be distinguished: "low-temperature" and "high-temperature". It has been suggested that in the low-temperature range, the quadratic dependence of the conductivity in a magnetic field might be associated with the "electron-phonon-surface" interference scattering mechanism.
3. The analysis of data on the Hall effect in $MoTe_2$ was carried out using single-band and two-band models. The values of concentration and mobility of current carriers were estimated. The Hall coefficients calculated from both models are in good agreement. Apparently, the two-band model is preferable in such systems containing different groups of current carriers.

Author Contributions: Conceptualization, V.V.M.; methodology, V.V.M., A.N.P. and S.V.N.; formal analysis, V.V.M., A.N.P. and S.V.N.; investigation, A.N.P.; resources, S.V.N.; data curation, V.V.M. and A.N.P.; writing—original draft preparation, A.N.P.; writing—review and editing, V.V.M. and S.V.N.; visualization, A.N.P.; supervision, V.V.M.; funding acquisition, V.V.M. All authors have read and agreed to the published version of the manuscript.

Funding: The results of studies of electrical resistivity (Section 3.1) were obtained within the state assignment of the Ministry of Science and Higher Education of the Russian Federation (theme "Spin," No. 122021000036-3), supported in part by the scholarship of the President of the Russian Federation to young scientists and graduate students (A.N.P., SP-2705.2022.1). Studies of magnetoresistivity (Section 3.2) and the Hall effect (Section 3.3) were supported by the Russian Science Foundation (project no. 22-42-02021).

Data Availability Statement: The data presented in this study are available on request from the corresponding author.

Acknowledgments: The authors thank S.M. Podgornykh, V.V. Chistyakov, and E.B. Marchenkova for help in the measurements and study of the structure of the sample.

Conflicts of Interest: The authors declare no conflict of interest.

References

1. Armitage, N.P.; Mele, E.J.; Vishwanath, A. Weyl and Dirac semimetals in three-dimensional solids. *Rev. Mod. Phys.* **2018**, *90*, 015001. [CrossRef]
2. Lv, B.Q.; Qian, T.; Ding, H. Experimental perspective on three-dimensional topological semimetals. *Rev. Mod. Phys.* **2021**, *93*, 025002. [CrossRef]

3. Hasan, M.Z.; Kane, C.L. Colloquium: Topological insulators. *Rev. Mod. Phys.* **2010**, *82*, 3045–3067. [CrossRef]
4. Liu, Y.; Chong, C.; Chen, W.; Huang, J.A.; Cheng, C.; Tsuei, K.; Li, Z.; Qiu, H.; Marchenkov, V.V. Growth and characterization of MBE-grown $(Bi_{1-x}Sb_x)_2Se_3$ topological insulator. *Jpn. J. Appl. Phys.* **2017**, *56*, 070311. [CrossRef]
5. Yan, B.; Felser, C. Topological Materials: Weyl Semimetals. *Annu. Rev. Condens. Matter Phys.* **2017**, *8*, 337–354. [CrossRef]
6. Xu, S.-Y.; Belopolski, I.; Alidoust, N.; Neupane, M.; Bian, G.; Zhang, C.; Sankar, R.; Chang, G.; Yuan, Z.; Lee, C.-C.; et al. Discovery of a Weyl Fermion semimetal and topological Fermi arcs. *Science* **2015**, *349*, 613–617. [CrossRef]
7. Soluyanov, A.A.; Gresch, D.; Wang, Z.; Wu, Q.; Troyer, M.; Dai, X.; Bernevig, B.A. Type-II Weyl semimetals. *Nature* **2015**, *527*, 495–498. [CrossRef]
8. Wu, Y.; Mou, D.; Jo, N.H.; Sun, K.; Huang, L.; Bud'ko, S.L.; Canfield, P.C.; Kaminski, A. Observation of Fermi arcs in the type-II Weyl semimetal candidate WTe_2. *Phys. Rev. B* **2016**, *95*, 121113. [CrossRef]
9. Wang, C.; Zhang, Y.; Huang, J.; Nie, S.; Liu, G.; Liang, A.; Zhang, Y.; Shen, B.; Liu, J.; Hu, C.; et al. Observation of Fermi arc and its connection with bulk states in the candidate type-II Weyl semimetal WTe_2. *Phys. Rev. B* **2016**, *94*, 241119. [CrossRef]
10. Sun, Y.; Wu, S.-C.; Ali, M.N.; Felser, C.; Yan, B. Prediction of Weyl semimetal in orthorhombic $MoTe_2$. *Phys. Rev. B* **2015**, *92*, 161107. [CrossRef]
11. Deng, K.; Wan, G.; Deng, P.; Zhang, K.; Ding, S.; Wang, E.; Yan, M.; Huang, H.; Zhang, H.; Xu, Z.; et al. Experimental observation of topological Fermi arcs in type-II Weyl semimetal $MoTe_2$. *Nat. Phys.* **2016**, *12*, 1105–1110. [CrossRef]
12. Chernozatonskii, L.A.; Artukh, A.A. Quasi-two-dimensional transition metal dichalcogenides: Structure, synthesis, properties and applications. *Phys. Usp.* **2018**, *61*, 2. [CrossRef]
13. Kim, H.-J.; Kang, S.-H.; Hamada, I.; Son, Y.-W. Origins of the structural phase transitions in $MoTe_2$ and WTe_2. *Phys. Rev. B* **2017**, *95*, 180101. [CrossRef]
14. Vellinga, M.B.; de Jonge, R.; Haas, C. Semiconductor to Metal Transition in $MoTe_2$. *J. Solid State Chem.* **1970**, *2*, 299–302. [CrossRef]
15. Clarke, R.; Marseglia, E.; Hughes, H.P. A low-temperature structural phase transition in β-$MoTe_2$. *Philos. Mag. B* **1978**, *38*, 121–126. [CrossRef]
16. Ali, M.N.; Xiong, J.; Flynn, S.; Tao, J.; Gibson, Q.D.; Schoop, L.M.; Liang, T.; Haldolaarachchige, N.; Hirschberger, M.; Ong, N.P.; et al. Large, non-saturating magnetoresistance in WTe_2. *Nature* **2014**, *514*, 205–208. [CrossRef]
17. Keum, D.H.; Cho, S.; Kim, J.H.; Choe, D.-H.; Sung, H.-J.; Kan, M.; Kang, H.; Hwang, J.-Y.; Kim, S.W.; Yang, H.; et al. Bandgap opening in few-layered monoclinic $MoTe_2$. *Nat. Phys.* **2015**, *11*, 482–486. [CrossRef]
18. Li, P.; Wen, Y.; He, X.; Zhang, Q.; Xia, C.; Yu, Z.-M.; Yang, S.A.; Zhu, Z.; Alshareef, N.H.; Zhang, X.-X. Evidence for topological type-II Weyl semimetal WTe_2. *Nat. Commun.* **2017**, *8*, 2150. [CrossRef] [PubMed]
19. Shekhar, C.; Nayak, A.K.; Sun, Y.; Schmidt, M.; Nicklas, M.; Leermakers, I.; Zeitler, U.; Skourski, Y.; Wosnitza, J.; Liu, Z.; et al. Extremely large magnetoresistance and ultrahigh mobility in the topological Weyl semimetal candidate NbP. *Nat. Phys.* **2015**, *11*, 645–649. [CrossRef]
20. Liang, T.; Gibson, Q.; Ali, M.N.; Liu, M.; Cava, R.J.; Ong, N.P. Ultrahigh mobility and giant magnetoresistance in the Dirac semimetal Cd_3As_2. *Nat. Mater.* **2015**, *14*, 280–284. [CrossRef]
21. Zandt, T.; Dwelk, H.; Janowitz, C.; Manzke, R. Quadratic temperature dependence up to 50 K of the resistivity of metallic $MoTe_2$. *J. Alloys Compd.* **2007**, *442*, 216–218. [CrossRef]
22. Chen, F.C.; Lv, H.Y.; Luo, X.; Lu, W.J.; Pei, Q.L.; Lin, G.T.; Han, Y.Y.; Zhu, X.B.; Song, W.H.; Sun, Y.P. Extremely large magnetoresistance in the type-II Weyl semimetal $MoTe_2$. *Phys. Rev. B* **2016**, *94*, 235154. [CrossRef]
23. Chen, F.C.; Luo, X.; Xiao, R.C.; Lu, W.J.; Zhang, B.; Yang, H.X.; Li, J.Q.; Pei, Q.L.; Shao, D.F.; Zhang, R.R.; et al. Superconductivity enhancement in the S-doped Weyl semimetal candidate $MoTe_2$. *Appl. Phys. Lett.* **2016**, *108*, 162601. [CrossRef]
24. Lv, Y.-Y.; Cao, L.; Li, X.; Zhang, B.-B.; Wang, K.; Pang, B.; Ma, L.; Lin, D.; Yao, S.-H.; Zhou, J.; et al. Composition and temperature dependent phase transition in miscible $Mo_{1-x}W_xTe_2$ single crystals. *Sci. Rep.* **2017**, *7*, 44587. [CrossRef] [PubMed]
25. Perevalova, A.N.; Naumov, S.V.; Podgornykh, S.M.; Chistyakov, V.V.; Marchenkova, E.B.; Fominykh, B.M.; Marchenkov, V.V. Kinetic properties of topological semimetal WTe_2 single crystal. *Phys. Met. Metallogr.* 2022, 123, *in press*.
26. Kaveh, M.; Cherry, M.F.; Weger, M. New mechanism for the electrical resistivity of layer compounds: TiS_2. *J. Phys. C Solid State Phys.* **1981**, *14*, L789–L795. [CrossRef]
27. Zhou, Q.; Rhodes, D.; Zhang, Q.R.; Tang, S.; Schonemann, R.; Balicas, L. Hall effect within the colossal magnetoresistive semimetallic state of $MoTe_2$. *Phys. Rev. B* **2016**, *94*, 121101. [CrossRef]
28. Lee, S.; Jang, J.; Kim, S.I.; Jung, S.-G.; Kim, J.; Cho, S.; Kim, S.W.; Rhee, J.Y.; Park, K.-S.; Park, T. Origin of extremely large magnetoresistance in the candidate type-II Weyl semimetal $MoTe_{2-x}$. *Sci. Rep.* **2018**, *8*, 13937. [CrossRef]
29. Levy, F. Single-crystal growth of layered crystals. *II Nuovo Cim. B* **1977**, *38*, 359–368. [CrossRef]
30. Brown, B.E. The Crystal Structures of WTe_2 and High-Temperature $MoTe_2$. *Acta Cryst.* **1966**, *20*, 268–274. [CrossRef]
31. Al-Hilli, A.A.; Evans, B.L. The preparation and properties of transition metal dichalcogenide single crystals. *J. Cryst. Growth* **1972**, *15*, 93–101. [CrossRef]
32. Bhattarai, N.; Forbes, A.W.; Dulal, R.P.; Pegg, I.L.; Philip, J. Transport characteristics of type II Weyl semimetal MoTe2 thin films grown by chemical vapor deposition. *J. Mater. Res.* **2020**, *35*, 454–461. [CrossRef]
33. Startsev, V.E.; D'yakina, V.P.; Cherepanov, V.I.; Volkenshtein, N.V.; Nasyrov, R.S.; Manakov, V.G. Quadratic temperature dependence of the resistivity of tungsten single crystals. Role of surface scattering of electrons. *Sov. Phys. JETP* **1980**, *52*, 675–679.

34. Marchenkov, V.V. Quadratic temperature dependence of magnetoresistivity of pure tungsten single crystals under static skin effect. *Low Temp. Phys.* **2011**, *37*, 852–855. [CrossRef]
35. Marchenkov, V.V.; Weber, H.W. Size Effect in the High-Field Magnetoconductivity of Pure Metal Single Crystals. *J. Low Temp. Phys.* **2003**, *132*, 135–144. [CrossRef]
36. Luo, Y.; Li, H.; Dai, Y.M.; Miao, H.; Shi, Y.G.; Ding, H.; Taylor, A.J.; Yarotski, D.A.; Prasankumar, R.P.; Thompson, J.D. Hall effect in the extremely large magnetoresistance semimetal WTe_2. *Appl. Phys. Lett.* **2015**, *107*, 182411. [CrossRef]